

# Gravito-diamagnetic forces for mass independent large spatial superpositions

Run Zhou,<sup>1</sup> Ryan J. Marshman,<sup>2</sup> Sougato Bose,<sup>3</sup> and Anupam Mazumdar<sup>1</sup>

<sup>1</sup>*Van Swinderen Institute, University of Groningen, 9747 AG Groningen, The Netherlands.*

<sup>2</sup>*Centre for Quantum Computation and Communication Technology, School of Mathematics and Physics, University of Queensland, Brisbane, Queensland 4072, Australia*

<sup>3</sup>*Department of Physics and Astronomy, University College London, Gower Street, WC1E 6BT London, United Kingdom.*

(Dated: May 1, 2023)

Testing the quantum nature of gravity in a laboratory via entanglement requires us to create a massive spatial quantum superposition, i.e. the Schrödinger cat state, where the mass and the superposition ought to be around  $10^{-15} - 10^{-14}$  kg and  $\Delta x \sim 10 - 100$   $\mu\text{m}$ . Creating such a massive spatial quantum superposition poses incredible challenges. The methods employed so far rely either on wavepacket expansion or on a quantum ancilla, e.g. single spin dependent forces, which scale inversely with mass. In this paper, we will show that gravitational acceleration along with the diamagnetic repulsion can achieve a complete “release” and “catch” interferometry in the course of which a large spatial superposition is generated in a relatively short time. After first creating a modest initial spatial superposition 1  $\mu\text{m}$  (e.g. using Stern-Gerlach), we will show that we can achieve an  $\sim 10^3$  fold improvement to the spatial superposition size (1  $\mu\text{m} \rightarrow 980$   $\mu\text{m}$ ) between the wave packets in less than 0.02 s by using the Earth’s gravitational acceleration and then the diamagnetic repulsive scattering of the nanocrystal, neither of which depend on the object mass. Finally, the wave packet trajectories can be closed so that spatial interference fringes can be observed or spin coherence can be further recovered using the SG apparatus.

**Introduction:** Gravity could be a classical, or an emergent, or a quantum entity [1]. There is no experimental proof to ascertain the quantum nature of gravity in a laboratory [2]. It is pertinent to ask how to show the quantum nature of gravity in a laboratory. Recently the quantum protocol has been established to explore the quantum origin of gravity with the help of quantum superposition and quantum entanglement in the infrared [3–6], see also for a similar proposal [7]. Note that the entanglement is inherently a quantum entity, and has no classical analogue. A protocol is known as the quantum gravity induced entanglement of masses (QGEM), which evidences both quantum superposition of geometries [8, 9], and the exchange of massless spin-2 graviton [5, 6, 10], that is, the massless excitation of spin-2 graviton. A protocol has also been created to entangle the matter with that of the Standard Model photon in a gravitational optomechanical setup [11], see also [12], which probes the light bending due to the gravitational interaction and also constrain the spin-2 nature of the graviton mediated entanglement [11].

To realise the QGEM protocol experimentally is extremely challenging, we will need to create a large spatial superposition  $\Delta x \sim O(10-100)$   $\mu\text{m}$  for a large mass object  $m \sim O(10^{-15} - 10^{-14})$  kg, see for details in [3, 13] in a free falling setup [3, 14]. Creating a macroscopic quantum superposition has many other fundamental applications; testing very foundation of quantum mechanics in presence of gravity [15–19], equivalence principle [20], placing the bound on the decoherence mechanisms [21–27], quantum sensors [14, 28], probing fifth force [29], and detecting gravitational waves [28]. Atom interferometers have already created a large baseline superposition [30–32],

but at masses well below what is required to test the quantum nature of gravity. To date, macromolecules represent the heaviest masses placed in a superposition of spatially distinct states [33, 34]. There are many physical schemes to obtain tiny superpositions of large masses [35] for 10 nm – 1  $\mu\text{m}$  superposition for  $m \sim 10^{-19} - 10^{-17}$  kg [22, 23, 36–48]. However, the QGEM proposal requires a large spatial superposition and heavy masses. For this reason the scheme will likely be utilising the Stern-Gerlach (SG) effect [49–51]. A proof of principle experiment has already been performed using atoms [52]. However, the critical challenge is how to achieve a large spatial superposition, and whether it is possible to benefit from Earth’s gravitational acceleration when creating the superposition.

There are already a couple of experimental schemes for creating large spatial superposition state for massive objects [52–54], but these schemes inevitably become progressively less effective as the mass increases. However, we have recently shown that it is possible to provide a mass-independent scheme to enhance the spatial superposition from the initial superposition size of  $\sim 1$   $\mu\text{m}$  with the help of diamagnetic repulsion [55]. However, the final spatial superposition size that can be achieved and the running time required is related to the initial velocity of the diamond. The larger the initial velocity, the larger will be the superposition size and the shorter the running time will be. However, in [55], we faced a challenge to obtain a large initial velocity for a massive diamond in a short time due to the configuration as assumed. We assumed that the experiment would be performed in a drop tower facility where we could neglect the Earth’s gravity. In this paper, we will relax this assumption,

and we will also modify the configuration in such a way as to overcome the challenge of obtaining a large initial velocity. As a consequence, we will also obtain an enhancement in the size of the superposition in a shorter time scale, in this regard the current paper is entirely a new design for creating a massive, large spatial superposition via diamagnetic repulsion.

This paper will aim to illustrate how such a mass-independent scheme of diamagnetic repulsion can benefit by utilising Earth's gravitational acceleration in a unique way to create even quicker enhancement of  $\mathcal{O}(980) \mu\text{m}$  in 0.02 s. This current scheme has many advantages compared to the earlier methods of creating a large spatial superposition, e.g. [42, 53–55]. Although the diamagnetic repulsion scheme remains the foundation of both the current and the paper [55], where it was first analysed for the case of creating a large spatial superposition, we believe that this paper's application will be extremely important in realising the QGEM experiment in less than 1 s<sup>1</sup>. Further note, that we will only consider the enhancement scheme here; we will assume that initially, the spatial superposition splitting of  $\mathcal{O}(1)\mu\text{m}$  has already been created by other known mechanisms, such as [38, 42, 53, 54, 56].

**Mass-independent acceleration:** We assume that the experimental apparatus is fixed in the Earth's gravitational field. The Hamiltonian of a diamond with a nitrogen-vacancy (NV) centre spin embedded in presence of an external magnetic field is given by: [38, 42, 53, 56]

$$\hat{H} = \frac{\hat{\mathbf{p}}^2}{2m} + \hbar D \hat{S}_{z'}^2 - \hat{\mu} \cdot \mathbf{B} + mg\hat{\mathbf{z}} - \frac{\chi_\rho m}{2\mu_0} \mathbf{B}^2. \quad (1)$$

The first term in Eq.(1) represents the kinetic energy of the diamond,  $\hat{\mathbf{p}}$  is the momentum operator and  $m$  is the mass of the diamond. The second term represents the zero-field splitting of the NV centre with  $D = (2\pi) \times 2.8 \text{ GHz}$ ,  $\hbar$  is the reduced Planck constant and  $\hat{S}_{z'}$  is the spin component operator aligned with the NV axis. The third term represents the interaction energy of the NV electron spin magnetic moment with the magnetic field  $\mathbf{B}$ . Spin magnetic moment operator  $\hat{\mu} = -g_s \mu_B \hat{\mathbf{S}}$ , where  $g_s \approx 2$  is the Landé g-factor,  $\mu_B = e\hbar/2m_e$  is the Bohr magneton and  $\hat{\mathbf{S}}$  is the NV spin operator. The fourth term is the gravitational potential energy,  $g \approx 9.8 \text{ m/s}^2$  is the gravitational acceleration and  $\hat{\mathbf{z}}$  is the position operator along the direction of gravity ( $z$  axis). The final term represents the magnetic energy of a

diamagnetic material (diamond) in a magnetic field,  $\chi_\rho = -6.2 \times 10^{-9} \text{ m}^3/\text{kg}$  is the mass susceptibility and  $\mu_0$  is the vacuum permeability.

We first assume that the initial superposition state is  $|+\rangle = (|m_s = +1\rangle + |m_s = -1\rangle)/\sqrt{2}$  with spatial splitting  $\Delta x_0$ .  $m_s$  is the NV spin quantum number. Then apply a microwave  $\pi/2$  pulse to convert  $|+\rangle$  to  $|m_s = 0\rangle$  state [57, 58] thus the spin magnetic field interaction can be ignored. Therefore, by neglecting the spin magnetic field interaction, the potential energy in Eq.(1) reduces to:

$$U = mg\hat{\mathbf{z}} - \frac{\chi_\rho m}{2\mu_0} \mathbf{B}^2. \quad (2)$$

To facilitate the separation of the wave packets by using the diamagnetic repulsion, we will consider the central magnetic field generated by the current-carrying wire

$$\mathbf{B} = \frac{\mu_0 \mathbf{I} \times \mathbf{e}_r}{2\pi r}, \quad (3)$$

where  $\mathbf{I}$  is the current carried by a straight wire.  $r$  is the radius from a point in space to the centre of the wire.  $\mathbf{e}_r$  is the unit vector corresponding to the radius  $r$ . Combining Eq.(2) and Eq.(3), we can obtain the acceleration of the diamond as follows

$$\mathbf{a}_{dia} = -\frac{1}{m} \nabla U = -g\mathbf{e}_z + \alpha \frac{I^2}{r^3} \mathbf{e}_r, \quad (4)$$

where

$$\alpha = -\frac{\chi_\rho \mu_0}{4\pi^2}. \quad (5)$$

$\mathbf{e}_z$  is the unit vector along the positive  $z$  axis. Note that Eq.(4) the acceleration is independent of the mass. This property provides an excellent possibility of obtaining a large superposition size for a massive quantum object. If we define the straight wire be perpendicular to the  $x - z$  plane and take the diamond to start to fall from rest, then the motion of the diamond will be only in the  $x - z$  plane.

**Scattering processes:** The experimental scheme is divided into two stages (see Fig.1). The first stage (Stage-I) serves to enhance the spatial superposition. The second stage (Stage-II) is to close the trajectories of the wave packets and produce spatial interference. Stage-I is divided into two parts. The first part is to use the mass-independent gravitational acceleration to accelerate the diamond. By controlling the falling height one can control the speed of the diamond. The second part is to use the mass-independent diamagnetic acceleration (the second term on the right-hand side of Eq.(4)) to change the velocity direction of the diamond. If the initial positions of the two wave packets in the superposition are symmetric about the wire, then they can change their velocity direction in the opposite directions and thus a large spatial separation can be obtained, as shown in Fig.1. In Stage-II,

<sup>1</sup> Finishing the experiment in less than 1 s, or minimising the interaction time between the two interferometers has many advantages. This will further help us to mitigate gravity gradient and relative acceleration noise, along with the seismic noise. Of course, this aspect has to be clearly understood and goes beyond the current paper.

the two wave packets are scattered and change velocity direction by two left and right symmetrical wires and eventually their trajectories are closed.

We will show analytically the process by which the diamond is accelerated by the gravitational field and then scattered elastically by the magnetic field generated by the current-carrying wire, and then numerically calculate the trajectory of the wave packet to verify the analytical results.

**Analytical treatment:** We assume that the diamond is accelerated by gravity from the rest at a distance from the wire and the effect of diamagnetic repulsion on the diamond can be ignored at the initial stages of the free-fall. We set the distance  $z_0$  at which the diamond is accelerated by gravity. The initial velocity of the diamond derived by the gravitational acceleration is given by

$$\mathbf{v}_{in} = \sqrt{2z_0 g} \mathbf{e}_z. \quad (6)$$

The time for the diamond to fall from its initial position to the splitting wire is

$$t_1 = \sqrt{\frac{2z_0}{g}}. \quad (7)$$

We now consider the process of a diamond incident at a velocity  $\mathbf{v}_{in}$ , and then scattered by the magnetic field generated by the current-carrying wire. This scattering process can be solved analytically, see [55]. The scattering angle of the diamond scattered by the central magnetic field is given by [55]

$$\theta_s = \left(1 - \frac{1}{\sqrt{k}}\right)\pi, \quad (8)$$

where

$$k = 1 + \alpha \frac{I^2}{v_{in}^2 b^2}. \quad (9)$$

Here  $b$  is the impact parameter. The geometric picture of  $\theta_s$  and  $b$  is shown in Fig.1. In order to obtain the maximum superposition size in the shortest time, we set the scattering angle for the first time  $\theta_{s1} = \pi/2$ . We assume that the diamond is scattered for the second time at coordinates  $(\pm x_{spl}, z_1)$  with the left (right) wire, and that the velocity direction after scattering is parallel to the  $x$ -axis. If  $x_{spl} = z_0$ , then the scattering angle for the second time  $\theta_{s2} \approx 3\pi/4$ . The time for the diamond to travel from splitting wire to left (right) wire is

$$t_2 = \frac{x_{spl}}{v_x}. \quad (10)$$

$v_x$  is the component of the velocity of the diamond along the  $x$ -axis. Since the scattering angle is  $\pi/2$ , therefore  $v_x = v_{in}$ . And then the time for the diamond to travel from left (right) wire to  $z$ -axis is

$$t_3 = \frac{x_{spl}}{\sqrt{v_x^2 + g^2 t_2^2}}. \quad (11)$$

Combining Eq.(6), (7), (10) and (11) gives a total evolution time of

$$t_{tot} = t_1 + t_2 + t_3, \\ = \sqrt{\frac{2z_0}{g}} \left( 1 + \frac{x_{spl}}{2z_0} + \frac{x_{spl}}{\sqrt{4z_0^2 + x_{spl}^2}} \right). \quad (12)$$

It can be seen from Eq.(12) that when  $z_0$  is fixed, the smaller the  $x_{spl}$ , the shorter the evolution time  $t_{tot}$ . We have ignored the deceleration and acceleration of the diamond as it approaches the wire in our calculations. This is because the diamagnetic repulsion is inversely proportional to the third power of the distance and only dominates when the diamond is very close to the wire ( $\sim 10 \mu\text{m}$ ).

**Numerical results:** We use the equation of motion, Eq.(4), to numerically solve for the trajectory of the wave packet. The numerical results are shown in Fig.1. We set the initial separation between wave packets  $\Delta x_0 = 1 \mu\text{m}$  ( $b = 0.5 \mu\text{m}$ ) and the initial coordinates of the expectation values of the positions of the two wave packets to be  $(\pm 0.5, 490) \mu\text{m}$ . The coordinate of the splitting wire is  $(0, 0)$  and the current through it, which is determined by Eq.(8) with  $\theta_{s1} = \pi/2$ , is  $6.04138 \text{ A}$ . The coordinates of the left and right wires are  $(\pm 491, -122.6) \mu\text{m}$ . We adjust the currents in the left and right wires so that the velocity direction of the wave packet is approximately parallel to the  $x$ -axis after the second scattering. The current through the left and right wires are  $10 \text{ A}$ . All three wires are switched on during the experiment.

It is important to note that fluctuations in the current can affect the accuracy of the wave packet position (expectation value) and thus the spatial interference fringe. We analysed the effect of current fluctuations on the wave packet position and the limits imposed on current fluctuations in order to produce spatial interference in Appendix A.

With the parameters we have set, the total dynamical time agrees well between analytical and numerical results ( $0.0194742 \text{ s}$  vs.  $0.0194958 \text{ s}$ ). In the process of separating and then recombining the two wave packets, the maximum superposition size reaches about  $980 \mu\text{m}$  and the initial separation between the wave packets is amplified by a factor of about 1000.

The closest distance of the wave packet trajectory to the splitting wire is  $1.00081 \mu\text{m}$ , and the closest distance of the wavepacket to the left (right) wire is  $1.32289 \mu\text{m}$ . If this minimum distance is considered (as an upper limit) to be the maximum radius of the wire, then the current density is  $\sim 1.9 \text{ A}/\mu\text{m}^2$  for the splitting wire, and  $\sim 1.8 \text{ A}/\mu\text{m}^2$  for the left (right) wire, which is *currently* achievable in a laboratory with carbon nanotubes and graphene [59–61]. The current density through the wire,  $\rho_{current}$ , the incident velocity of the diamond,  $v_{in}$ , and the impact

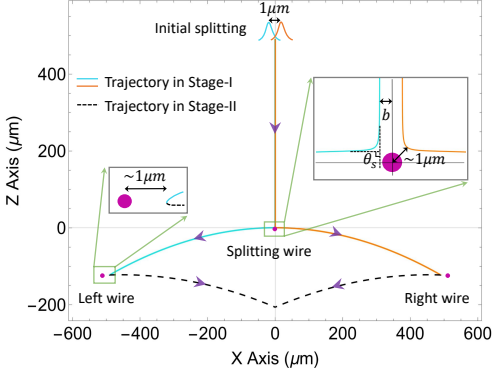


FIG. 1. Experimental scheme and numerical results for creating mass independent spatial superposition. The two wave packets with an initial spatial splitting of  $\Delta x_0$  start falling, *under Earth's gravity acting along the  $-z$  direction*, from the rest and enter the magnetic field generated by the current-carrying wires. The purple points represent straight wires perpendicular to the  $x - z$  plane. The wire at the origin is called the splitting wire located at  $(x = 0, z = 0)$ . The wire on the left is called the *left wire* and the wire on the right is called the *right wire*. The blue and orange solid lines represent the wave packet trajectory in stage-I and the black dashed lines represent the wave packet trajectory in stage-II. The purple arrows indicate the direction of motion of the wave packets. The sign  $b$  is the impact parameter and the initial splitting  $\Delta x_0 = 2b = 1 \mu\text{m}$ . The sign  $\theta_s$  is the scattering angle. The total motion time is around 0.0195 s.

parameter,  $b$ , satisfy [55]

$$\rho_{\text{current}} = \frac{I}{\pi d^2} = \frac{1}{b} \frac{C v_{in}^2}{\pi(v_{in}^2 + \alpha C^2)}, \quad (13)$$

where  $C = I/b$  and  $d$  is the closest distance of the wave packet trajectory to the centre of the wire. When the scattering angle is  $\pi/2$ , combining Eq.(8) and (13) and we then have

$$\rho_{\text{current}} = \frac{1}{4b\pi} \sqrt{\frac{3}{\alpha}} v_{in}. \quad (14)$$

From Eq.(14) it can be seen that the current density is linear with the incident velocity. Additionally, the current density is also inversely proportional to the impact parameter  $b$ . This means that for a smaller initial separation ( $\Delta x_0 = 2b$ ), we will need a larger current density to achieve the same superposition size.

**Conclusion and discussion:** In this paper we have achieved  $\sim 1000$  times increment in the spatial superposition, from  $1 \mu\text{m} \rightarrow 980 \mu\text{m}$  between the wave packets in 0.02 s by using gravitational acceleration and the repulsive, diamagnetic scattering off the diamond. There are three distinct advantages to this scheme. (1) The first is that the process of enhancing the spatial superposition is *mass independent*. In the ideal situation, when all the known Standard Model interactions are under control along with all the known sources of the decoherence, we can use

this mass-independent scheme to increase the spatial superposition between the wave packets  $\mathcal{O}(10^3) \mu\text{m}$ , or even higher, provided that we can create an initial spatial superposition, even one as small as  $1 \mu\text{m}$  or less<sup>2</sup>. This scheme solves some of the outstanding challenges of creating large spatial superposition, either using the wave packet expansions [22, 33, 34, 44–48] or spin-dependent forces [52–54]. In all the previous cases the efficacy is reduced by any increase in the mass. (2) The second advantage is that the whole process takes a shorter time (around 0.02 s) compared to previous schemes for creating large spatial superposition [42, 53, 54]. The shorter time in which one experimental run is performed will reduce the time during which the environment can act to decohere the system. This will also improve the total run-time of the experiment or conversely increase the number of experimental runs performed which is essential for witnessing the entanglement induced by the quantum nature of gravity [24, 25]. (3) The third advantage is that the experimental apparatus (wires) is fixed. Compared to the previous scheme of creating spatial superposition [53–55], where the experimental apparatus is free falling in the gravitational field, this is easier to achieve in the laboratory. It is also possible to create spatial superposition in optical or magnetic levitation systems [62, 63], but the levitation system itself limits the superposition size that can be achieved.

It is important to note that although the process of enhancing the superposition size is mass independent, there are two factors that limit the mass of the diamond. The first is that an initial spatial splitting between wave packets is required. If the SG apparatus is used to split the wave packet, the process of creating the initial spatial splitting is still mass dependent [53, 54]. The second is that the distance between the diamond and the wire limits the mass of the diamond. If the maximum radius of the diamond is assumed to be half the minimum distance between the diamond and the wire ( $\sim 0.5 \mu\text{m}$ ), this corresponds to a maximum diamond mass of approximately  $10^{-15} \text{ kg}$ .

In this scheme, the separation and closing of the wave packet trajectories can be achieved using a modest current density  $\mathcal{O}(1) \text{ A}/\mu\text{m}^2$ . The ability to close the wave packet trajectories means that we can use the SG apparatus to completely recombine the trajectories of the wave packets and eventually recover spin coherence [53, 54]. The latter aspects will be discussed separately. In addition to these, there are

<sup>2</sup> Our scheme works even for a smaller initial separation, i.e. for  $\Delta x_0 \sim 0.2 \mu\text{m}$ , a value that could potentially be achieved by a spin dynamical decoupling method for a diamond with a mass of  $10^{-17} \text{ kg}$ , see [42]. We can still obtain almost the same maximum superposition size of about  $\sim 1000 \mu\text{m}$ , by a reasonable current density of about  $10 \text{ A}/\mu\text{m}^2$ .

other issues, such as coherence of the spin in presence of the NV centre [64], or the excitations of the phonons [65]. However, such considerations are left for future study. Since this diamagnetic enhancement does not itself require any spin-based manipulation, there may be simpler candidate for creating (and closing) the initial small spatial splitting which does not concern itself with the issues of rotation. However it will likely that similar constraints may arise to ensure

coherent interference is possible.

**Acknowledgements** R. Z. is supported by China Scholarship Council (CSC) fellowship. R. J. M. is supported by the Australian Research Council (ARC) under the Centre of Excellence for Quantum Computation and Communication Technology (CE170100012). S. B. would like to acknowledge EPSRC grants (EP/N031105/1, EP/S000267/1 and EP/X009467/1) and grant ST/W006227/1.

---

[1] F. DYSON, Is a graviton detectable?, *International Journal of Modern Physics A* **28**, 1330041 (2013).

[2] A. Addazi *et al.*, Quantum gravity phenomenology at the dawn of the multi-messenger era—A review, *Prog. Part. Nucl. Phys.* **125**, 103948 (2022), arXiv:2111.05659 [hep-ph].

[3] S. Bose, A. Mazumdar, G. W. Morley, H. Ulbricht, M. Toroš, M. Paternostro, A. A. Geraci, P. F. Barker, M. Kim, and G. Milburn, Spin entanglement witness for quantum gravity, *Physical Review letters* **119**, 240401 (2017).

[4] [https://www.youtube.com/watch?v=0Fv-0k13s\\_k](https://www.youtube.com/watch?v=0Fv-0k13s_k) (2016), accessed 1/11/22.

[5] R. J. Marshman, A. Mazumdar, and S. Bose, Locality and entanglement in table-top testing of the quantum nature of linearized gravity, *Physical Review A* **101**, 052110 (2020).

[6] S. Bose, A. Mazumdar, M. Schut, and M. Toroš, Mechanism for the quantum natured gravitons to entangle masses, *Physical Review D* **105**, 106028 (2022).

[7] C. Marletto and V. Vedral, Gravitationally induced entanglement between two massive particles is sufficient evidence of quantum effects in gravity, *Physical Review Letters* **119**, 240402 (2017).

[8] M. Christodoulou and C. Rovelli, On the possibility of laboratory evidence for quantum superposition of geometries, *Physics Letters B* **792**, 64 (2019).

[9] M. Christodoulou, A. Di Biagio, M. Aspelmeyer, Č. Brukner, C. Rovelli, and R. Howl, Locally mediated entanglement through gravity from first principles, arXiv preprint arXiv:2202.03368 (2022).

[10] D. L. Danielson, G. Satishchandran, and R. M. Wald, Gravitationally mediated entanglement: Newtonian field versus gravitons, *Physical Review D* **105**, 086001 (2022).

[11] D. Biswas, S. Bose, A. Mazumdar, and M. Toroš, Gravitational Optomechanics: Photon-Matter Entanglement via Graviton Exchange, (2022), arXiv:2209.09273 [gr-qc].

[12] D. Carney, Newton, entanglement, and the graviton, *Phys. Rev. D* **105**, 024029 (2022), arXiv:2108.06320 [quant-ph].

[13] T. W. van de Kamp, R. J. Marshman, S. Bose, and A. Mazumdar, Quantum Gravity Witness via Entanglement of Masses: Casimir Screening, *Phys. Rev. A* **102**, 062807 (2020), arXiv:2006.06931 [quant-ph].

[14] M. Toroš, T. W. Van De Kamp, R. J. Marshman, M. S. Kim, A. Mazumdar, and S. Bose, Relative acceleration noise mitigation for nanocrystal matter-wave interferometry: Applications to entangling masses via quantum gravity, *Phys. Rev. Res.* **3**, 023178 (2021), arXiv:2007.15029 [gr-qc].

[15] R. Penrose, On gravity's role in quantum state reduction, *General relativity and gravitation* **28**, 581 (1996).

[16] L. Diósi, Continuous Quantum Measurement and Ito Formalism, *Phys. Lett. A* **129**, 419 (1988), arXiv:1812.11591 [quant-ph].

[17] P. Pearle, Combining stochastic dynamical state-vector reduction with spontaneous localization, *Physical Review A* **39**, 2277 (1989).

[18] A. Bassi, K. Lochan, S. Satin, T. P. Singh, and H. Ulbricht, Models of wave-function collapse, underlying theories, and experimental tests, *Reviews of Modern Physics* **85**, 471 (2013).

[19] S. Nimmrichter and K. Hornberger, Macroscopicity of mechanical quantum superposition states, *Physical Review Letters* **110**, 160403 (2013).

[20] S. Bose, A. Mazumdar, M. Schut, and M. Toroš, Entanglement Witness for the Weak Equivalence Principle, (2022), arXiv:2203.11628 [gr-qc].

[21] O. Romero-Isart, Quantum superposition of massive objects and collapse models, *Phys. Rev. A* **84**, 052121 (2011).

[22] O. Romero-Isart, A. C. Pflanzer, F. Blaser, R. Kaltenbaek, N. Kiesel, M. Aspelmeyer, and J. I. Cirac, Large quantum superpositions and interference of massive nanometer-sized objects, *Physical Review Letters* **107**, 020405 (2011).

[23] O. Romero-Isart, M. L. Juan, R. Quidant, and J. I. Cirac, Toward quantum superposition of living organisms, *New Journal of Physics* **12**, 033015 (2010).

[24] J. Tilly, R. J. Marshman, A. Mazumdar, and S. Bose, Qudits for witnessing quantum-gravity-induced entanglement of masses under decoherence, *Phys. Rev. A* **104**, 052416 (2021), arXiv:2101.08086 [quant-ph].

[25] M. Schut, J. Tilly, R. J. Marshman, S. Bose, and A. Mazumdar, Improving resilience of quantum-gravity-induced entanglement of masses to decoherence using three superpositions, *Phys. Rev. A* **105**, 032411 (2022), arXiv:2110.14695 [quant-ph].

[26] S. Rijavec, M. Carlesso, A. Bassi, V. Vedral, and C. Marletto, Decoherence effects in non-classicality tests of gravity, *New J. Phys.* **23**, 043040 (2021), arXiv:2012.06230 [quant-ph].

[27] D. Carney, P. C. E. Stamp, and J. M. Taylor, Tabletop experiments for quantum gravity: a user's manual, *Classical and Quantum Gravity* **36**, 034001 (2019).

[28] R. J. Marshman, A. Mazumdar, G. W. Morley, P. F. Barker, S. Hoekstra, and S. Bose, Mesoscopic Interference for Metric and Curvature (MIMAC) & Gravitational Wave Detection, *New J. Phys.* **22**, 083012 (2020), arXiv:1807.10830 [gr-qc].

[29] P. F. Barker, S. Bose, R. J. Marshman, and A. Mazumdar, Entanglement based tomography to probe new macroscopic forces, *Phys. Rev. D* **106**, L041901 (2022), arXiv:2203.00038 [hep-ph].

[30] J. M. McGuirk, G. T. Foster, J. B. Fixler, M. J. Snadden, and M. A. Kasevich, Sensitive absolute-gravity gradiometry using atom interferometry, *Physical Review A* **65**, 033608 (2002).

[31] S. Dimopoulos, P. W. Graham, J. M. Hogan, and M. A. Kasevich, General relativistic effects in atom interferometry, *Physical Review D* **78**, 042003 (2008).

[32] P. Asenbaum, C. Overstreet, T. Kovachy, D. D. Brown, J. M. Hogan, and M. A. Kasevich, Phase shift in an atom interferometer due to spacetime curvature across its wave function, *Physical Review Letters* **118**, 183602 (2017).

[33] M. Arndt, O. Nairz, J. Vos-Andreae, C. Keller, G. van der Zouw, and A. Zeilinger, Wave-particle duality of  $C_{60}$  molecules, *Nature* **401**, 680 (1999).

[34] S. Gerlich, S. Eibenberger, M. Tomandl, S. Nimmrichter, K. Hornberger, P. J. Fagan, J. Tüxen, M. Mayor, and M. Arndt, Quantum interference of large organic molecules, *Nature communications* **2**, 1 (2011).

[35] S. Bose, K. Jacobs, and P. L. Knight, A Scheme to probe the decoherence of a macroscopic object, *Phys. Rev. A* **59**, 3204 (1999), arXiv:quant-ph/9712017.

[36] P. Sekatski, M. Aspelmeyer, and N. Sangouard, Macroscopic optomechanics from displaced single-photon entanglement, *Physical Review Letters* **112**, 080502 (2014).

[37] J. M. Hogan, D. Johnson, and M. A. Kasevich, Light-pulse atom interferometry, arXiv preprint arXiv:0806.3261 (2008).

[38] C. Wan, M. Scala, G. Morley, A. A. Rahman, H. Ulbricht, J. Bateman, P. Barker, S. Bose, and M. Kim, Free nano-object ramsey interferometry for large quantum superpositions, *Physical Review Letters* **117**, 143003 (2016).

[39] M. Scala, M. S. Kim, G. W. Morley, P. F. Barker, and S. Bose, Matter-wave interferometry of a levitated thermal nano-oscillator induced and probed by a spin, *Physical Review Letters* **111**, 180403 (2013).

[40] Z.-q. Yin, T. Li, X. Zhang, and L. Duan, Large quantum superpositions of a levitated nanodiamond through spin-optomechanical coupling, *Physical Review A* **88**, 033614 (2013).

[41] J. Clarke and M. R. Vanner, Growing macroscopic superposition states via cavity quantum optomechanics, *Quantum Science and Technology* **4**, 014003 (2019).

[42] B. D. Wood, S. Bose, and G. W. Morley, Spin dynamical decoupling for generating macroscopic superpositions of a free-falling nanodiamond, *Physical Review A* **105**, 012824.

[43] J. S. Pedernales, G. W. Morley, and M. B. Plenio, Motional Dynamical Decoupling for Interferometry with Macroscopic Particles, *Physical Review Letters* **125**, 023602 (2020).

[44] R. Kaltenbaek, M. Aspelmeyer, P. F. Barker, A. Bassi, J. Bateman, K. Bongs, S. Bose, C. Braxmaier, Č. Brukner, B. Christophe, et al., Macroscopic quantum resonators (maqro): 2015 update, *EPJ Quantum Technology* **3**, 5 (2016).

[45] H. Pino, J. Prat-Camps, K. Sinha, B. P. Venkatesh, and O. Romero-Isart, On-chip quantum interference of a superconducting microsphere, *Quantum Science and Technology* **3**, 025001 (2018).

[46] O. Romero-Isart, Coherent inflation for large quantum superpositions of levitated microspheres, *New Journal of Physics* **19**, 123029 (2017).

[47] R. Kaltenbaek, G. Hechenblaikner, N. Kiesel, O. Romero-Isart, K. C. Schwab, U. Johann, and M. Aspelmeyer, Macroscopic quantum resonators (maqro), *Experimental Astronomy* **34**, 123 (2012).

[48] M. Arndt and K. Hornberger, Testing the limits of quantum mechanical superpositions, *Nature Physics* **10**, 271 (2014).

[49] S. Machluf, Y. Japha, and R. Folman, Coherent stern-gerlach momentum splitting on an atom chip, *Nature Communications* **4**, 2424 (2013).

[50] O. Amit, Y. Margalit, O. Dobkowski, Z. Zhou, Y. Japha, M. Zimmermann, M. A. Efremov, F. A. Narducci, E. M. Rasel, W. P. Schleich, and R. Folman,  $T^3$  stern-gerlach matter-wave interferometer, *Physical Review Letters* **123**, 083601 (2019).

[51] Y. Margalit, Z. Zhou, O. Dobkowski, Y. Japha, D. Rohrlich, S. Moukouri, and R. Folman, Realization of a complete stern-gerlach interferometer, arXiv preprint arXiv:1801.02708 (2018).

[52] Y. Margalit, O. Dobkowski, Z. Zhou, O. Amit, Y. Japha, S. Moukouri, D. Rohrlich, A. Mazumdar, S. Bose, C. Henkel, and R. Folman, Realization of a complete stern-gerlach interferometer: Toward a test of quantum gravity, *Science Advances* **7**, 10.1126/sci-adv.2879 (2021).

[53] R. J. Marshman, A. Mazumdar, R. Folman, and S. Bose, Constructing nano-object quantum superpositions with a Stern-Gerlach interferometer, *Phys. Rev. Res.* **4**, 023087 (2022), arXiv:2105.01094 [quant-ph].

[54] R. Zhou, R. J. Marshman, S. Bose, and A. Mazumdar, Catapulting towards massive and large spatial quantum superposition, *Physical Review Research* **4**, 043157 (2022), arXiv:2206.04088 [quant-ph].

[55] R. Zhou, R. J. Marshman, S. Bose, and A. Mazumdar, Mass Independent Scheme for Large Spatial Quantum Superpositions, (2022), arXiv:2210.05689 [quant-ph].

[56] J. S. Pedernales, G. W. Morley, and M. B. Plenio, Motional dynamical decoupling for interferometry with macroscopic particles, *Physical Review Letters* **125**, 023602 (2020).

[57] J. M. Taylor, P. Cappellaro, L. Childress, L. Jiang, D. Budker, P. R. Hemmer, A. Yacoby, R. Walsworth, and M. D. Lukin, High-sensitivity diamond magnetometer with nanoscale resolution, *Nature Physics* **4**, 810 (2008).

[58] E. V. Levine, M. J. Turner, P. Kehayias, C. A. Hart, N. Langellier, R. Trubko, D. R. Glenn, R. R. Fu, and R. L. Walsworth, Principles and techniques of the quantum diamond microscope, *Nanophotonics* **8**, 1945 (2019).

- [59] Z. Yao, C. L. Kane, and C. Dekker, High-field electrical transport in single-wall carbon nanotubes, *Physical Review Letters* **84**, 2941 (2000).
- [60] B. Q. Wei, R. Vajtai, and P. M. Ajayan, Reliability and current carrying capacity of carbon nanotubes, *Applied Physics Letters* **79**, 1172 (2001).
- [61] R. Murali, Y. Yang, K. Brenner, T. Beck, and J. D. Meindl, Breakdown current density of graphene nanoribbons, *Applied Physics Letters* **94**, 243114 (2009).
- [62] U. Delić, M. Reisenbauer, K. Dare, D. Grass, V. Vuletić, N. Kiesel, and M. Aspelmeyer, Cooling of a levitated nanoparticle to the motional quantum ground state, *Science* **367**, 892 (2020).
- [63] J.-F. Hsu, P. Ji, C. W. Lewandowski, and B. D'Urso, Cooling the Motion of Diamond Nanocrystals in a Magneto-Gravitational Trap in High Vacuum, *Scientific Reports* **6**, 30125 (2016).
- [64] Y. Japha and R. Folman, Role of rotations in stern-gerlach interferometry with massive objects 10.48550/arxiv.2202.10535 (2022).
- [65] C. Henkel and R. Folman, Internal decoherence in nano-object interferometry due to phonons, *AVS Quantum Sci.* **4**, 025602 (2022), arXiv:2112.01263 [quant-ph].
- [66] Y. Margalit, Z. Zhou, S. Machluf, Y. Japha, S. Moukouri, and R. Folman, Analysis of a high-stability Stern–Gerlach spatial fringe interferometer, *New Journal of Physics* **21**, 073040 (2019).
- [67] S. Machluf, Y. Japha, and R. Folman, Coherent Stern–Gerlach momentum splitting on an atom chip, *Nature Communications* **4**, 2424 (2013).
- [68] B. R. Slezak, C. W. Lewandowski, J.-F. Hsu, and B. D'Urso, Cooling the motion of a silica microsphere in a magneto-gravitational trap in ultra-high vacuum, *New Journal of Physics* **20**, 063028 (2018).

## Appendices

### Appendix A LIMITATION OF CURRENT FLUCTUATION

Fluctuations in the current, according to Eq.(4), can induce classical uncertainties in the position and momentum of the object, thus affecting spatial interference [66], momentum interference [67] and spin coherence [51] between wave packets. As the diamond collides elastically with the wire and the wire is fixed, fluctuations in current only influence the direction but not the magnitude of the velocity of the diamond. Therefore, we are only discussing here the deviation in the spatial position of the diamond. To focus on the effect of current fluctuations on the trajectory, we assume that there are no errors in the classical position and momentum of the diamond at the initial moment.

We now calculate the deviation of the trajectory of the diamond after first scattering and second scattering with the wire, respectively, when there is a small current fluctuation  $\Delta I$ . To simplify the calculation,

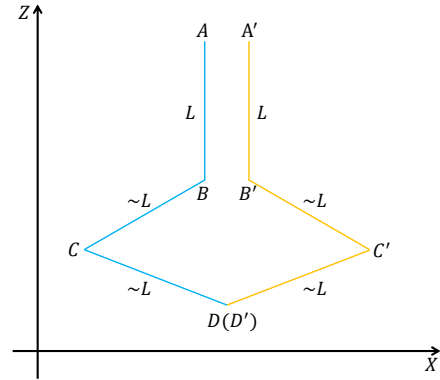


FIG. 2. The sketch of the wave packet trajectories.

we assume that the trajectory of the diamond consists of different line segments and that the length of each segment is  $L$ , as shown in Fig.2. As the trajectories of the left and right wave packets are symmetrical, we use the left trajectory (blue line segment) for illustration.

Using the expression for the scattering angle in Eq.(8) to differentiate the current and impact parameter gives

$$\begin{aligned}\Delta\theta_s &= \beta \left( \frac{\Delta I}{I} - \frac{\Delta b}{b} \right), \\ &= \Delta\theta_{sI} + \Delta\theta_{sb},\end{aligned}\quad (15)$$

where  $\Delta\theta_{sI} = \beta\Delta I/I$  is the change in scattering angle due to current fluctuation and  $\Delta\theta_{sb} = -\beta\Delta b/b$  is the change in scattering angle due to fluctuation in impact parameter.  $\beta$  is a coefficient related to the current  $I$ , the incident velocity  $v_{in}$  and the impact parameter  $b$ , with the expression

$$\beta = \frac{k-1}{k^{\frac{3}{2}}} \pi. \quad (16)$$

The expression for  $k$  is given in Eq.(9). For the first scattering, the scattering angle  $\theta_{s1} \approx \pi/2$ , and then  $\beta_1 = 3\pi/8$ . For the second scattering, the scattering angle  $\theta_{s2} \approx 3\pi/4$ , and then  $\beta_2 = 15\pi/64$ . According to Eq.(15), the classical trajectory deviation of the wave packet when it reaches point  $C$  can be written as

$$\Delta b_1 \approx \Delta\theta_{sI}(B) \times L = \beta_1 \frac{\Delta I}{I} L. \quad (17)$$

“ $B$ ” in brackets indicates fluctuations in the scattering angle at point  $B$ , similarly thereafter. Combining Eq.(15) and Eq.(17) gives the uncertainty in the scattering angle at the second scattering

$$\begin{aligned}\Delta\theta_s(C) &= \Delta\theta_{sI}(C) + \Delta\theta_{sb}(C), \\ &= \beta_1 \frac{\Delta I}{I} - \beta_1 \beta_2 \frac{\Delta I}{I} \frac{L}{b}.\end{aligned}\quad (18)$$

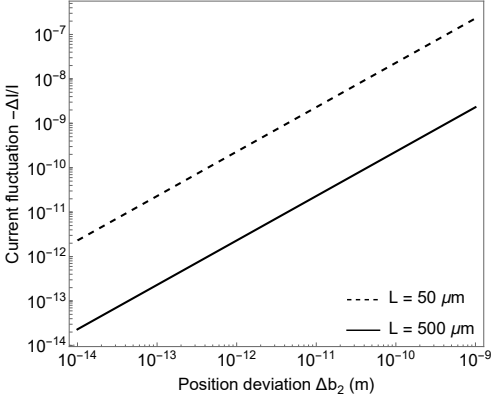


FIG. 3. Current fluctuation versus position deviation of the wave packet (at point  $D$ ). The black dashed line corresponds to  $L = 50 \mu\text{m}$  and the black solid line corresponds to  $L = 500 \mu\text{m}$ .  $L$  is defined in Fig.2. We set  $b = 5 \times 10^{-7} \text{ m}$ .

When  $L \gg b$  ( $\beta_2 \approx 0.7$ ), then  $\Delta\theta_{sb}(C) \ll \Delta\theta_{si}(C)$ . So for the second scattering we only consider  $\Delta\theta_{sb}(C)$ . When the wave packet reaches point  $D$ , the deviation of the classical trajectory is

$$\Delta b_2 \approx \Delta\theta_{sb}(C) \times L = -\beta_1 \beta_2 \frac{\Delta I}{I} \frac{L^2}{b}. \quad (19)$$

Rewrite Eq.(19) as

$$-\frac{\Delta I}{I} = \frac{b}{\beta_1 \beta_2 L^2} \Delta b_2. \quad (20)$$

If the two wave packets are required to interfere spatially at point  $D(D')$ , then  $\Delta b_2$  needs to be smaller than the corresponding wave packet width, which places a limit on the fluctuation of the current. Based on Eq.(20) we plot the relationship between current fluctuation  $\Delta I/I$  and position deviation  $\Delta b_2$  as shown in Fig.3. We can see that when the final requirement for position deviation is the same, the reduction in  $L$  (superposition size) by one order of magnitude reduces the requirement for current stability by two orders of magnitude.

Let us give a specific example to calculate the limits on current fluctuations. Consider a silica microsphere with a mass of  $10^{-15} \text{ kg}$  captured by a magnetic field with a frequency of 100 Hz [68]. The initial width of the wave packet is

$$\delta x = \sqrt{\frac{\hbar}{2m\omega}} \approx 2 \times 10^{-11} \text{ m}. \quad (21)$$

In order to produce spatial interference,  $\Delta b_2$  needs to be smaller than  $\delta x$ . Combining Eq.(20) and Eq.(21) we get

$$\left| \frac{\Delta I}{I} \right| \lesssim \begin{cases} 5 \times 10^{-11} & \text{for } L = 500 \mu\text{m}, \\ 5 \times 10^{-9} & \text{for } L = 50 \mu\text{m}. \end{cases} \quad (22)$$

However, since the wave packet evolves with time, the limits on current fluctuations will be less demanding than those given by Eq.(22).